Available online at www.sciencedirect.com
ScienceDirect
Trans. Nonferrous Met. Soc. China 31(2021) 3762−3771
Transactions of Nonferrous Metals Society of China
www.tnmsc.cn

Solidification behavior of Pt-containing 718Plus superalloy

Yu SHEN[1,2,3*], Min-qing WANG[3*], Hui XIA[1], Lei ZHENG[1], Ye MENG[4], Feng-e CUI[4]

1. School of Materials Science and Engineering, University of Science and Technology Beijing, Beijing 100083, China;
2. Gaona Aero Material Co., Ltd., Beijing 100081, China;
3. Superalloy Department, Central Iron and Steel Research Institute, Beijing 100081, China;
4. Institute of Advanced Materials and Technology,
University of Science and Technology Beijing, Beijing 100083, China

Received 7 November 2020; accepted 20 June 2021

Abstract: Solidification behaviors of Pt-containing 718Plus superalloys were studied by scanning electron microscopy (SEM), energy dispersive spectrum (EDS), differential scanning calorimetry (DSC) and simulation calculations. It is found that Pt increases solidification range and decreases solidus temperature of the alloy and precipitation temperature of Laves + γ eutectic phase since Pt enlarges the region of γ phase by increasing Nb solubility. In addition, Pt segregates to the interdendritic region and increases the segregation of Nb and Ti in the interdendritic region due to the strong attractive interactions between Pt and Nb/Ti. As a result, Pt promotes the precipitation of the Laves + γ eutectic phase and η phase around eutectic phase. The increase of solidification range and segregation degrees of Nb and Al caused by Pt also promotes the precipitation and growth of $\gamma' + \gamma''$ phase around eutectic phase. These results provide experimental bases for understanding the mechanism of Pt in solidification behavior of superalloys.

Key words: platinum; solidification behavior; 718Plus superalloy; eutectic

1 Introduction

With the continuous development of aero engines, the performance requirements at high temperature for anti-oxidation, anti-creep and long-term microstructure stability of the alloys are increasing significantly [1−4]. In order to improve the high-temperature strength and microstructure stability of the alloys, the concentration of refractory elements increased and new elements were introduced [5−7]. In 1980, CORTI et al [8] proposed the strategy of adding precious metal elements into nickel-based superalloys and found that the Pt-modified RJM alloys exhibit outstanding high-temperature strength, structural stability, oxidation resistance and anti-corrosion properties. In 2009, HEIDLOFF et al [9] found that Pt reduces the γ' phase coarsening kinetics and improves the γ' phase stability at 1000 °C of Ni−15Al−5Cr casting alloy. In 2015, SLUYTMANA et al [10] reported that PX5 casting alloy containing 2.5 at.% Pt displays exceptional high temperature microstructure stability at 1200 ℃ due to the lower diffusion coefficient of Pt in Ni.

As the types and concentrations of refractory elements and precious metal elements in super-alloys increase, the segregation degrees become severer due to their high mass fraction and low diffusivity [11−13]. To properly control the segregation degrees, it is essential to understand the solidification behavior of elements. At present, the studies of precious metal elements on solidification behavior of nickel-based superalloys concentrate

Corresponding author: Lei ZHENG, Tel: +86-10-62332884, Fax: +86-10-62327283, E-mail: zhenglei_ustb@sina.com
* Yu SHEN and Min-qing WANG contributed equally to this work
DOI: 10.1016/S1003-6326(21)65762-X

into Ru and reveal that Ru reduces the segregation degrees of other alloying elements [14−16]. As for Pt, LIN et al [17] found that Pt segregates to interdendritic region, promotes the segregation of Al and Ta, and reduces the solidus, liquidus and eutectic temperatures of single crystal superalloy. However, studies on the role of Pt in the solidification behavior of polycrystalline superalloys have not been reported until now. Therefore, the present work is carried out to investigate the solidification behavior of Pt-containing 718Plus superalloy, including the solidification structure, dendrite spacing, eutectic phase and element segregation characteristics.

2 Experimental

The chemical compositions of experimental alloys are listed in Table 1. The base alloy used is ATI 718Plus alloy, which is newly developed polycrystalline nickel-based superalloy and is designed for using in modern aero engine compressor discs as a replacement for Inconel 718 alloy [18−20]. The 718Plus-0Pt and 718Plus-1.5Pt alloy (in wt.%) ingots, weighing approximately 3 kg, were prepared by the same vacuum induction melting to minimize oxidation and then chill cast in a cylindrical copper mold, with a conical hot top section to accommodate shrinkage within the casting.

A disk with 3 mm in thickness and 60 mm in diameter was cut from each ingot at the center, 1/2 radius (1/2*R*) and edge position. Metallographic observations were performed after the samples were ground and polished. Subsequently, samples were etched in a solution of 150 mL H_3PO_4 + 10 mL H_2SO_4 + 15 g CrO_3. Microstructural observations were conducted with optical microscopy (OM). The secondary dendritic arm spacing was measured by Photoshop image analysis software. The microstructure at high magnification was observed on a scanning electron microscope (SEM). Qualitative chemical analyses of precipitates were performed by the energy-dispersive spectrometer (EDS) equipped with the SEM. Five points were taken among the interdendritic and dendritic cores and averaged.

Differential scanning calorimetry (DSC) measurements were performed to estimate the transformation temperatures of phases. The samples were cut from the center of the ingots with the size of 6 mm in diameter and 7 mm in thickness, along with a countersink of 7.5 mm^2 (2.5 mm × 3 mm) at one end. DSC experiments were conducted on a high-purity argon atmosphere to avoid oxidation. The samples were subjected to heating and cooling cycles as follows: room temperature → heating at 20 °C/min up to 1000 °C → isothermal holding at 1000 °C for 20 min → heating at 5 °C/min up to 1450 °C → isothermal holding at 1450 °C for 20 min → cooling at 5 °C/min down to 1000 °C → cooling at 20 °C/min down to room temperature. Because the transformation of phases almost occurred in the temperature range of 1000−1450 °C [21], only the data within this interval were analyzed.

Using the JMatpro 7.0 software, thermodynamic calculations were employed to obtain the solidification sequence, the thermodynamic phase diagrams under simulated non-equilibrium solidification and the element distribution in the solid and residual liquid during solidification. Elemental redistribution was calculated by the Schell−Gulliver model [22].

3 Results

3.1 Calculation of solidification path and solutes distribution during solidification

The thermodynamic phase diagrams of 718Plus-0Pt and 718Plus-1.5Pt alloys under simulated non-equilibrium solidification are shown in Fig. 1. It can be seen from Fig. 1(a) that the solidification of 718Plus-0Pt alloy starts with the crystallization of γ phase at the liquidus temperature of 1345 °C and terminates at the solidus temperature of 1120 °C. The precipitation temperature of MC carbide locates at 1235 °C. When the temperature

Table 1 Chemical compositions of 718Plus-0Pt and 718Plus-1.5Pt alloys (wt.%)

Alloy	Ni	Cr	Fe	Co	Nb	Mo	Al	W	Ti	Pt
718Plus-0Pt	51.65	18.02	9.8	9.02	5.54	2.72	1.45	1.00	0.78	0
718Plus-1.5Pt	50.74	17.81	9.68	8.98	5.52	2.70	1.46	1.01	0.72	1.36

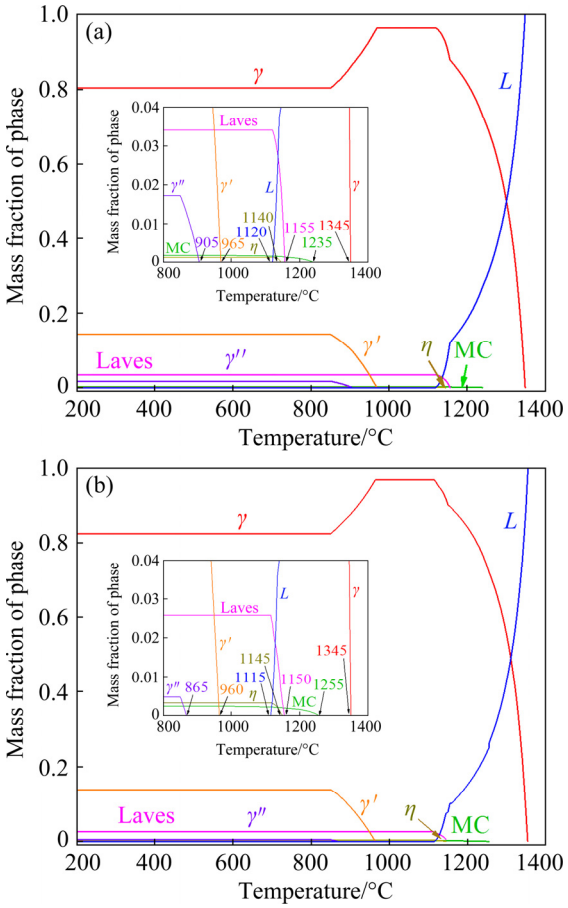

Fig. 1 Mass fractions of various phases as function of temperature during non-equilibrium solidification for both alloys: (a) 718Plus-0Pt; (b) 718Plus-1.5Pt

decreases to 1155 °C, Laves + γ eutectic structure forms. At 1140 °C, η phase precipitates from the γ matrix. Subsequently, the γ' and γ'' phases start to precipitate at 965 and 905 °C, respectively. It can be seen from Fig. 1(b) that the liquidus and solidus temperatures of 718Plus-1.5Pt alloy are 1345 and 1115 °C, respectively. The precipitation temperature of MC carbide is 1255 °C, and the Laves + γ eutectic structure forms at 1150 °C. At 1145 °C, η phase precipitates from the γ matrix. Whereafter, the γ' and γ'' phases start to precipitate at 960 and 865 °C, respectively. It is worth noting that the precipitation of metastable γ'' phase is caused by the non-equilibrium solidification process in 718Plus alloy [23].

It can be known that Pt decreases the solidus temperature, resulting in the increase of the solidification range. In addition, Pt reduces the precipitation temperature of Laves + γ eutectic phase. According to Fig. 1, the solidification paths of 718Plus-0Pt and 718Plus-1.5Pt alloys are identical, that is: $L \rightarrow L + \gamma \rightarrow L + \gamma + \text{MC} \rightarrow L + \gamma + \text{MC} + \text{Laves} \rightarrow L + \gamma + \text{MC} + \text{Laves} + \eta \rightarrow \gamma + \text{MC} + \text{Laves} + \eta + \gamma' \rightarrow \gamma + \text{MC} + \text{Laves} + \eta + \gamma' + \gamma''$. As a result, Pt does not change the solidification path and the type of precipitate phases of 718Plus alloy.

Figure 2 shows the calculated mass fractions of the elements in liquid versus solid fraction during the non-equilibrium solidification with the Schell−Gulliver model. It can be seen that the concentrations of negative segregation elements Cr, Fe, Co and W in liquid decrease generally as the solidification proceeds, while those of positive segregation elements Nb, Mo, Pt and Ti increase. In addition, Pt does not change the distribution tendency of other elements and has little influence on the concentrations of elements in the final liquid phase.

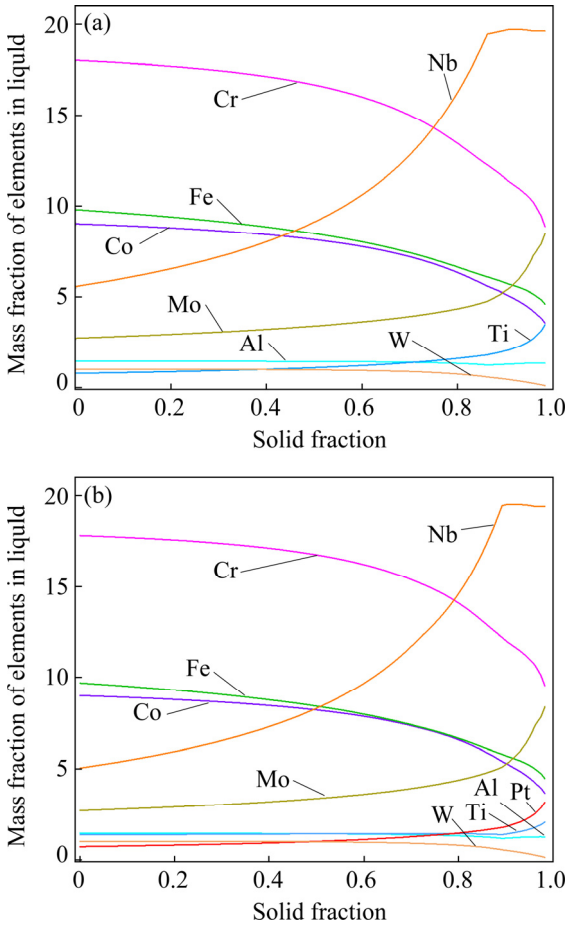

Fig. 2 Solutes distribution during solidification for both alloys: (a) 718Plus-0Pt; (b) 718Plus-1.5Pt

3.2 As-cast dendrite microstructure and secondary dendritic arm spacing

A typical dendritic microstructure including the dendritic core with higher lightness and the

interdendritic region with lower lightness are shown in Fig. 3. It can be seen that both alloys exhibit the same dendritic microstructure, and the dendritic cores consist of primary and secondary dendrites. The dendrite morphology at the edge of both ingots is columnar due to the faster directional heat dissipation conditions at the edges. The dendritic microstructure at the 1/2*R* and center positions exhibits a typical cross structure due to three-dimensional temperature field heating during the solidification [15,22].

As a critical microstructure parameter [24,25], the secondary dendrite arm spacing in different positions is shown in Fig. 4. It is demonstrated that the position with the largest secondary dendrite arm spacing of both alloys is the center, while the secondary dendrite arm spacing at the edge is reduced clearly. Compared with 718Plus-0Pt alloy, the secondary dendrite arm spacing of 718Plus-1.5Pt alloy at the same position is larger, indicating that Pt increases the degree of dendrite segregation.

3.3 Elemental segregation behavior

The degree of microsegregation between the dendrite core and interdendritic region is normally characterized with the segregation coefficient k [21]. The average segregation coefficient of each element at different locations for each alloy is recorded in Fig. 5. It is clear that segregation coefficients of Cr, Co, Fe, Al and W in both alloys are slightly less than 1, indicating that they segregate to the dendritic cores and their segregation degrees are low relatively. Nb, Mo, Ti, and Pt segregate in the interdendritic region and display positive segregation characteristics. Ni is almost evenly distributed in dendrite core and interdendritic region during solidification.

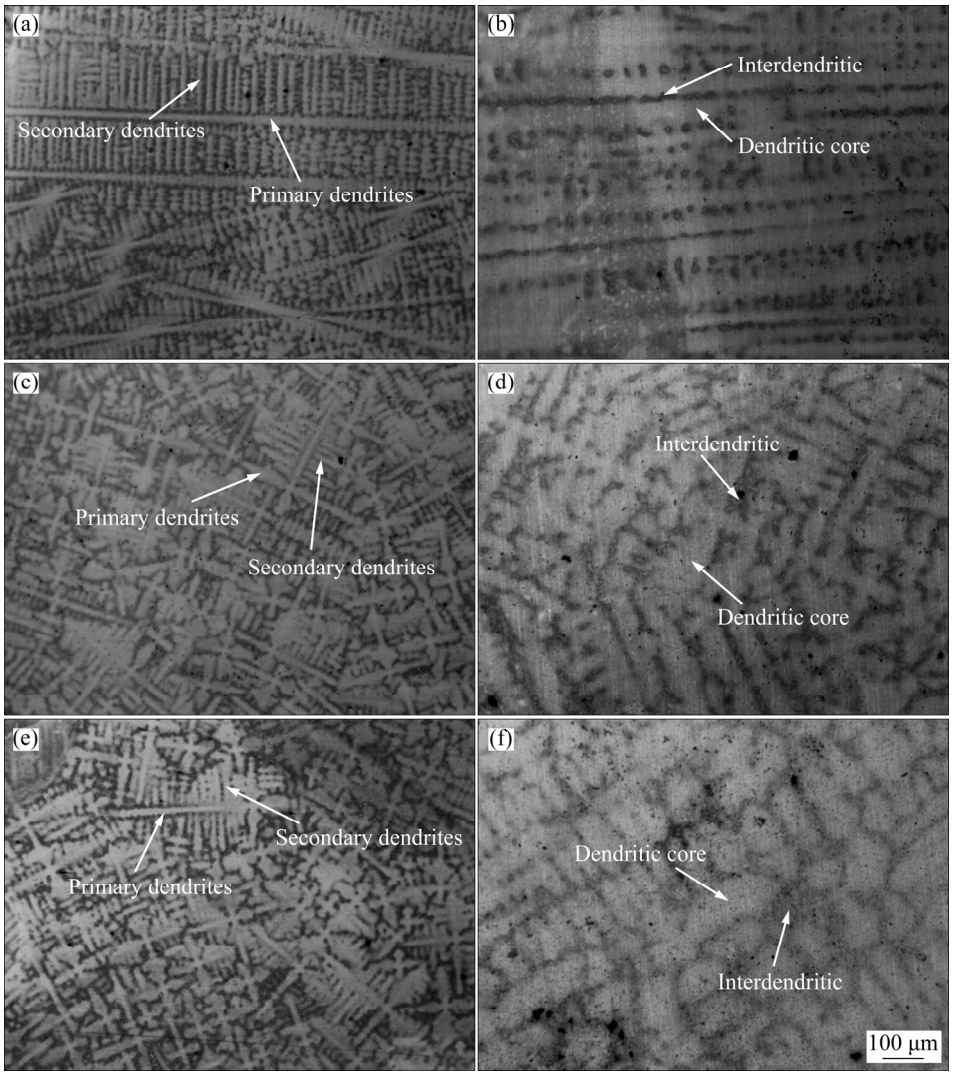

Fig. 3 Dendritic microstructures of both alloys: (a, c, e) Edge, middle (1/2*R*) and center of 718Plus-0Pt, respectively; (b, d, f) Edge, middle (1/2*R*) and center of 718Plus-1.5Pt, respectively

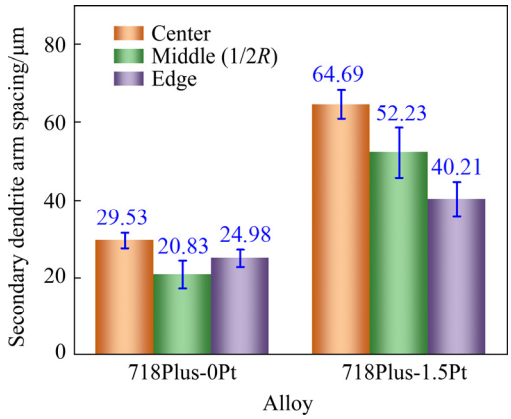

Fig. 4 Secondary dendrite arm spacing for both alloys

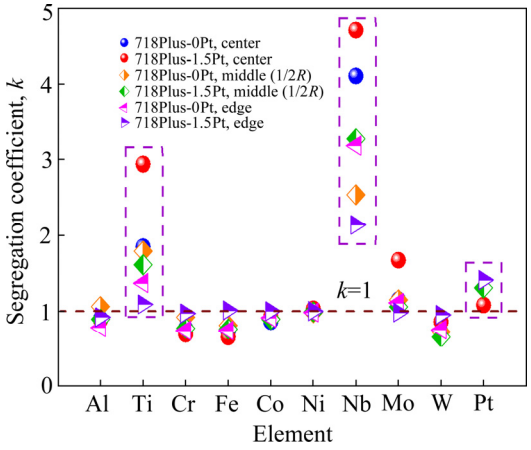

Fig. 5 Segregation coefficients of elements at different locations for both alloys

Through Fig. 5, it can be found that the segregation degree of Nb element is the highest and Ti is the second. For 718Plus-0Pt alloy, the highest segregation coefficients of Nb and Ti are 4.11 and 1.85, respectively. In contrast, the segregation coefficient of Nb in 718Plus-1.5Pt alloy is 4.71 and that of Ti is 2.94. It is obvious that Pt promotes the segregation of Nb and Ti and improves the segregation coefficients of these two elements.

3.4 Precipitation behavior of secondary phases in interdendritic region

During solidification, in addition to dendrite formation, different precipitates form in the interdendritic region due to element segregation. For example, a typical harmful TCP phase, i.e. Laves phase, will be produced due to the segregation of Nb element [26]. Figure 6 shows the microstructures of interdendritic region of both alloys. It can be seen from Figs. 6(a, b) that massive phases appear in the interdendritic region of both alloys. The SEM images of phase morphology at high magnification are shown in Figs. 6(c, d). The points marked with *A* and *B* in Figs. 6(c, d) are detected by EDS. The EDS results are shown in Fig. 7 and confirm the massive phases to be Laves phase rich in Nb and Mo. As well known, Laves phase forms due to the highly enriched Nb and Mo in the interdendritic region [27,28] and is often accompanied by γ phase to form the Laves + γ eutectic phase [19]. The morphology and solidification behavior of similar Laves + γ eutectic phase were also studied with the same method in other 718-type superalloys [29−31]. The Laves + γ eutectic phase is in chain-like shape and relatively dispersed in 718Plus-0Pt alloy (Fig. 6(a)), while that is in block-like shape and relatively aggregated in 718Plus-1.5Pt alloy with obvious increase in size (Fig. 6(b)). This means that Pt promotes the precipitation of Laves + γ eutectic phase.

It is observed that the needle-like phase exists around the eutectic phase (Fig. 6(d)). The composition of this needle-like phase (Point *C* in Fig. 6(f)) is detected by EDS. The composition of this phase is close to $Ni_3Al_{0.5}Nb_{0.5}$ [32], indicating that it is a η phase. It is obvious that there are more η phases around the Laves + γ eutectic phase in 718Plus-1.5Pt alloy, indicating that Pt promotes the precipitation of the η phase. Figures 6(e, f) show that there is also the flocculent $\gamma' + \gamma''$ phase around the Laves + γ eutectic phase in both alloys. This is consistent with the simulations during the non-equilibrium process in Fig. 1. In general, the needle-like η phase and floccular $\gamma' + \gamma''$ phase in 718Plus-1.5Pt alloy are significantly higher in amount than those in 718Plus-0Pt alloy.

3.5 Phase transition temperature

The DSC curves of both alloys during the heating and cooling processes are presented in Fig. 8. The solidus and liquidus temperatures are determined by the cooling and heating curves, respectively [21]. The solidus temperature T_S and liquidus temperature T_L of the 718Plus-0Pt alloy are 1306 and 1355 °C, respectively, and the solidification range T_L-T_S of the 718Plus-0Pt alloy is therefore 49 °C. The 718Plus-1.5Pt alloy exhibits a solidus temperature decreasing to 1297 °C and a liquidus temperature decreasing to 1353 °C. The solidification range of the 718Plus-1.5Pt alloy is enlarged to 56 °C. Besides, Fig. 8 displays an

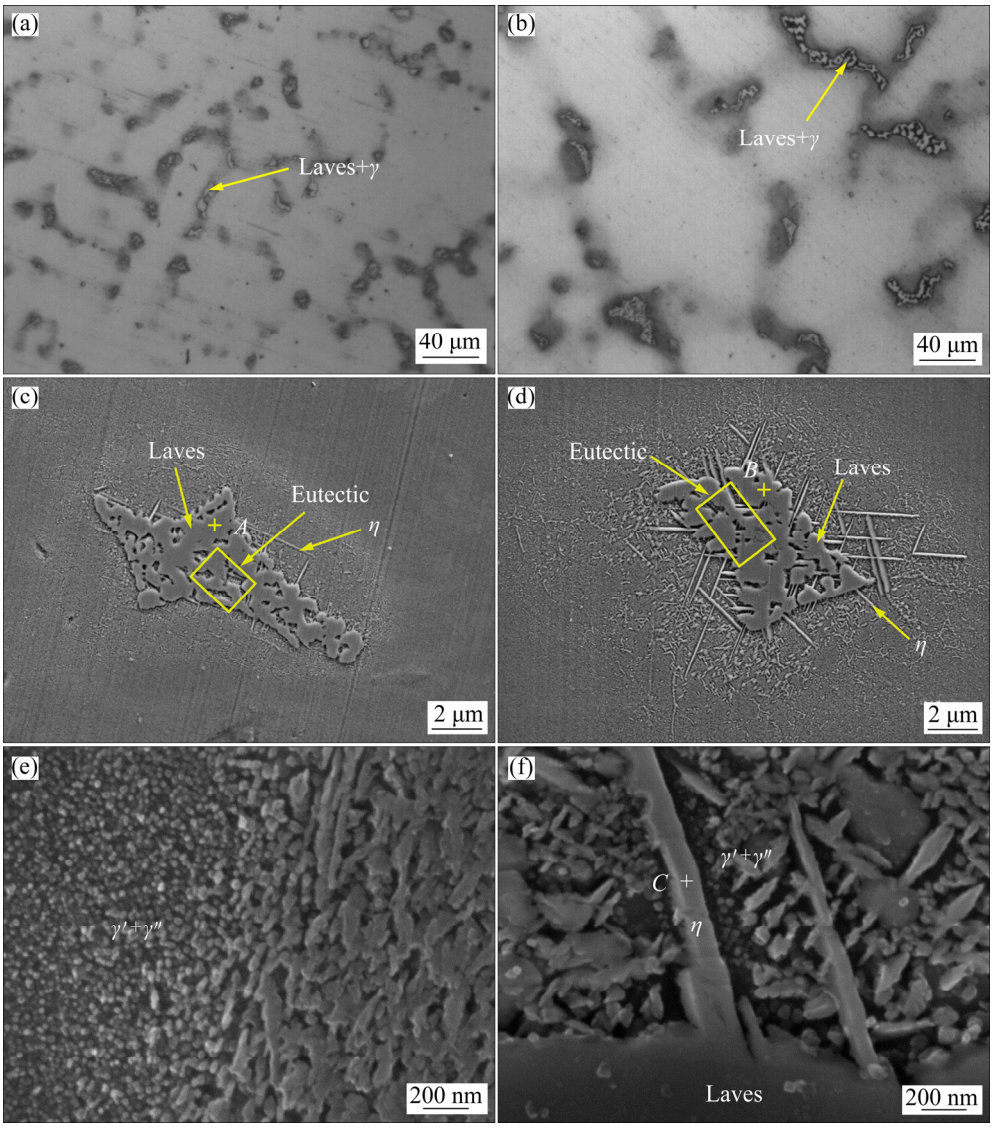

Fig. 6 Morphologies of different phases in center of both alloy ingots: (a, c, e) 718Plus-0Pt; (b, d, f) 718Plus-1.5Pt

obvious reaction peak for phase transformation in the cooling curves of both alloys. On these bases, the precipitation temperatures of the Laves + γ eutectic phase in 718Plus-0Pt and 718Plus-1.5Pt alloys are 1152 and 1149 °C, indicating that Pt reduces the precipitation temperatures of eutectic phase. The phase transition temperatures are summarized in Fig. 9.

4 Discussion

4.1 Promoted segregation of Nb and Ti

As illustrated by Figs. 1, 8 and 9, DSC measurement and thermodynamic calculation prove that Pt decreases solidus temperature and precipitation temperatures of the Laves + γ eutectic phase in 718Plus alloy and increases its solidification range. This phenomenon agrees well with previous research of LIN et al [17]. It is confirmed that Pt occupies the lattice sites of Ni and thus leads to the increase in the lattice of the γ phase due to the larger atomic radius of Pt [33,34]. Moreover, it is known from the pseudo-binary phase diagram [35] that Pt enlarges the region of γ phase by increasing Nb solubility. Thus, Pt increases solidification range of 718Plus alloy and decreases precipitation temperatures of the eutectic phase. In addition, the greater the solidification temperature range is, the longer the time for complete solidification is, and the severer the microsegregation is. Therefore, Pt increases the microsegregation during the solidification. This is also the reason that Pt increases the secondary dendrite arm spacing (see Fig. 4).

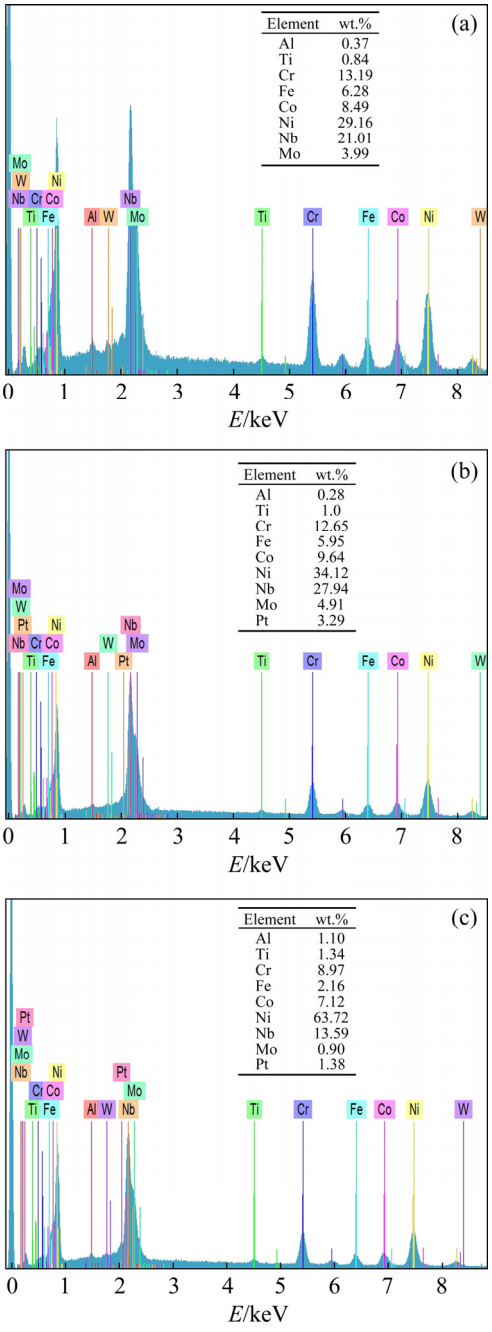

Fig. 7 EDS analyses of different phases in center of both alloy ingots: (a) Point *A* in Fig. 6(c); (b) Point *B* in Fig. 6(d); (c) Point *C* in Fig. 6(f)

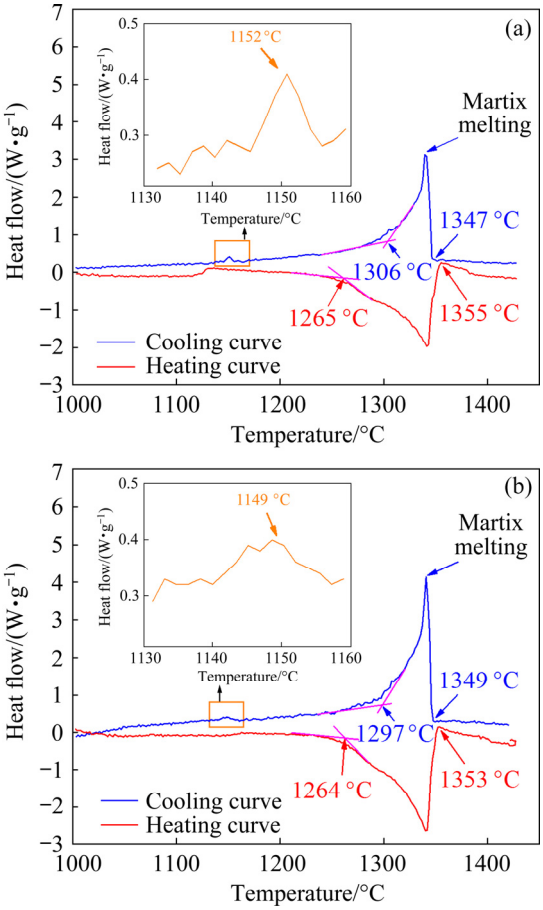

Fig. 8 DSC curves during heating and cooling processes for both alloys: (a) 718Plus-0Pt; (b) 718Plus-1.5Pt

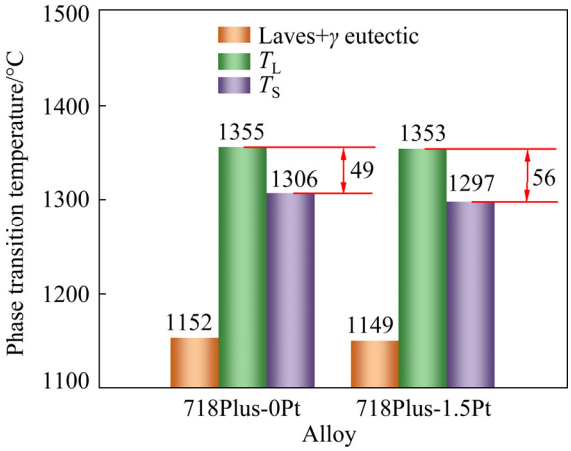

Fig. 9 Phase transition temperatures of both alloys

Figure 5 displays that segregation coefficients of Nb and Ti are much higher than those of Al, Cr, Fe, Co, Ni, Mo, and W. Besides, the segregation coefficients of Nb and Ti are promoted significantly by Pt. The chemical bonds of intermetallic compounds are basically metallic bonds, and the bonding energy is directly proportional to electronegativity difference [6]. According to the electronegativity value calculated by GHOSH and CHAKRABORTY [36], the electronegativity value of Pt is 7.72 eV, and that of Nb and Ti is 3.50 and 3.14 eV, respectively. Therefore, it is considered that Pt and Nb/Ti have strong binding energy. The strong binding energy between Pt and Nb can also be proved by the Nb−Pt binary phase diagrams, i.e. Nb_3Pt phase can be found in binary phase

diagrams [37,38]. Since Pt tends to segregate to the interdendritic region and has strong electronegativity, it attracts Nb and Ti to enrich in the interdendritic region and thus increases microsegregation degree of Nb and Ti elements.

4.2 Improvement of precipitation

The precipitation behaviors of the secondary phases in the interdendrite region exhibited in Fig. 6 display that Pt promotes the precipitation of the Laves + γ eutectic and η phases around eutectic phase. On the one hand, EDS results in Fig. 7 show that Pt exists in eutectic phase and η phase. This implies that Pt is a forming element of the two phases and promotes their precipitation inevitably. On the other hand, Pt promotes the segregation degrees of Nb and Ti in the interdendritic region. The accumulation of Pt, Nb and Ti promotes the precipitation of the Laves + γ eutectic and η phases naturally. It is worth noting that η phase often precipitates close to eutectic phase (see Figs. 6(c, d)). The EDS results in Fig. 7 demonstrate that both eutectic and η phases comprise high content of Nb, and Nb content in eutectic phase is even higher. In this case, when the eutectic phase grows, it consumes the Nb element nearby. Due to the slow diffusion of Nb [39,40], once the Nb content nearby is not high enough to facilitate the growth of the eutectic phase, η phase begins to nucleate at the eutectic/γ interface and grows.

Figures 6(e, f) illustrate that Pt increases the quantity of $\gamma' + \gamma''$ phase around eutectic phase. As preceding descriptions, the eutectic phase consumes Nb and Ti elements. At the same time, it discharges Al and Ni and aggravates the Al and Ni enrichment around eutectic phase. The accumulation of Al and Ni, combined with the remaining Nb, leads to the solidification of interdendritic Al-rich $\gamma' + \gamma''$ phase at the last stage of the solidification. Moreover, the increase in the solidification range caused by Pt allows more time for $\gamma' + \gamma''$ phase to precipitate and grow. In this case, $\gamma' + \gamma''$ phase has larger size and higher quantity.

4.3 Roles of Pt in solidification

Figure 10 shows the schematic diagram of the roles of Pt in the solidification of 718Plus alloy. Pt enlarges the region of γ phase by increasing Nb solubility, and thus decreases solidus temperature, increases solidification range and decreases precipitation temperature of eutectic phase. The increase in the solidification range promotes the secondary dendrite arm spacing and the segregation of Nb and Ti in the interdendritic region. Moreover, Pt segregates to the interdendritic region during the solidification and has strong electronegativity. Thus, it attracts Nb and Ti to enrich in the interdendritic region. In addition, Pt promotes the precipitation of the Laves + γ eutectic and η phases since Pt is the forming element of eutectic and η phases and promotes the segregation of Nb. The intensified Nb segregation and the increased solidification range give more time for $\gamma' + \gamma''$ phase to precipitate and grow.

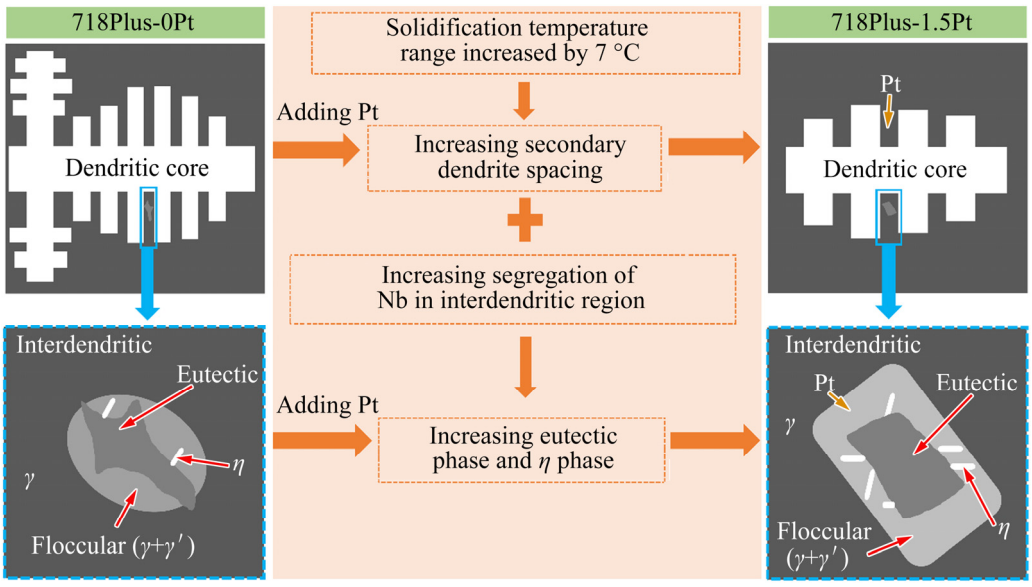

Fig. 10 Qualitative schematic diagram of roles of Pt in solidification

5 Conclusions

(1) Pt decreases solidus temperature, increases solidification range of the 718Plus alloy and decreases precipitation temperature of Laves + γ eutectic phase because Pt enlarges the region of γ phase by increasing Nb solubility.

(2) Pt segregates to the interdendritic region and increases the segregation degree of Nb and Ti in the interdendritic region due to the strong attractive interaction between Pt and Nb/Ti. Pt is the forming element of eutectic and η phases and thus promotes the precipitation of the Laves + γ eutectic and η phases around eutectic phase.

(3) The increase of solidification range and segregation degree of Nb, Al and Ni caused by Pt promotes the precipitation and growth of $\gamma' + \gamma''$ phase around eutectic phase.

Acknowledgments

The authors are grateful for the financial supports from the National Natural Science Foundation of China (Nos. 51771018, 51871022), and the Fundamental Research Funds for the Central Universities (Nos. FRF-GF-19-004B, FRF-GF-20-01A)

References

[1] XU Wen-liang, WANG Fu, MA De-xin, POLACZEK A B. Effect of Ru on macro-/micro-structure evolution within platform of Ni-based superalloy single crystal blades [J]. Journal of Alloys and Compounds, 2020, 817: 153337.

[2] LI Xin-xu, JIA Chong-lin, ZHANG Yong, LÜ Shao-min, JIANG Zhou-hua. Cracking mechanism in as-cast GH4151 superalloy ingot with high γ' phase content [J]. Transactions of Nonferrous Metals Society of China, 2020, 30: 2697−2708.

[3] ZHANG Hong-mei, GU Dong-dong, MA Cheng-long, GUO Meng, YANG Jian-kai, WANG Rui. Effect of post heat treatment on microstructure and mechanical properties of Ni-based composites by selective laser melting [J]. Materials Science and Engineering A, 2019, 765: 138294.

[4] SONAR T, MALARVIZHI S, BALASUBRAMANIAN V. Influence of arc constriction current frequency on tensile properties and microstructural evolution of tungsten inert gas welded thin sheets of aerospace alloy [J]. Transactions of Nonferrous Metals Society of China, 2021, 31: 456−474.

[5] SHI Zhen-xue, LI Jia-rong, LIU Shi-zhong, WANG Xiao-guang, YUE Xiao-dai. Effect of Ru on stress rupture properties of nickel-based single crystal superalloy at high temperature [J]. Transactions of Nonferrous Metals Society of China, 2012, 22: 2106−2111.

[6] GAO Shuang, ZHOU Yi-zhou, LI Cai-fu, LIU Zhi-Quan, JIN Tao. Effects of platinum group metals addition on the precipitation of topologically close-packed phase in Ni-base single crystal superalloys [J]. Journal of Alloys and Compounds, 2016, 671: 458−464.

[7] LI Ling-wei, YAN Mi. Recent progresses in exploring the rare earth based intermetallic compounds for cryogenic magnetic refrigeration [J]. Journal of Alloys and Compounds, 2020, 823: 85−92.

[8] CORTI C W, COUPLAND D R, SELMAN G L. Platinum-enriched superalloys [J]. Platinum Metals Review, 1980, 24: 2−11.

[9] HEIDLOFF A J, SLUYTMAN J V, POLLOCK T M, GLEESON B. Structural stability of platinum-group-metal-modified γ+γ' Ni-base alloys [J]. Metallurgical and Materials Transactions A, 2009, 40: 1529−1540.

[10] SLUYTMANA J S V, MOCERI C J, POLLOCK T M. A Pt-modified Ni-base superalloy with high temperature precipitate stability [J]. Materials Science and Engineering A, 2015, 639: 747−754.

[11] SEO S M, JEONG H W, AHM Y K, YUN D W, LEE J H, YOO Y S. Comparative study of quantitative micro-segregation analyses performed during the solidification of the Ni-base superalloy CMSX-10 [J]. Materials Characterization, 2014, 89: 43−55.

[12] YANG Cong, XU Qing-yan, SU Xiang-lin, LIU Bai-cheng. Multiphase-field and experimental study of solidification behavior in a nickel-based single crystal superalloy [J]. Acta Materialia, 2019, 175: 286−296.

[13] XIONG Zhi-ping, KOSTRYZHEV A G, STANFORD N E, PERELOMA E V. Microstructures and mechanical properties of dual phase steel produced by laboratory simulated strip casting [J]. Materials Design, 2015, 88: 537−549.

[14] ZHENG L, GU C Q, ZHENG Y R. Investigation of the solidification behavior of a new Ru-containing cast Ni-base superalloy with high W content [J]. Scripta Materialia, 2004, 50: 435−439.

[15] GUAN Ying-shuang, LIU En-ze, GUAN Xiu-rong, ZHENG Zhi. Influence of Ru on solidification behavior, microstructure and hardness of Re-free Ni-based equiaxed superalloys with high Cr content [J]. Journal of Materials Science and Technology, 2016, 32: 271−281.

[16] WANG Hai-feng, SU Hai-jun, ZHANG Jun, GUO min, ZHANG Yan-bin, YUE Quan-zhao, LIU Lin, HUANG Tai-wen, YANG Wen-chao, FU Heng-zhi. Investigation on solidification path of Ni-based single crystal superalloys with different Ru contents [J]. Materials Characterization, 2017, 130: 211−218.

[17] LIN Hui-wen, ZHOU Yi-zhou, ZHANG Xuan, JIN Tao, SUN Xiao-feng. Solidification behavior of a Pt-containing Ni-based single crystal superalloy [J]. Acta Metallurgica Sinica, 2013, 49: 1567−1572.

[18] WANG Min-qing, DU Jin-hui, DENG Qun, TIAN Zhi-ling, ZHU Jing. The effect of phosphorus on the microstructure and mechanical properties of ATI 718Plus alloy [J]. Materials Science and Engineering A, 2015, 626: 382−389.

[19] SINGH S, HANNING F, ANDERSSON J. Influence of homogenisation treatments on the hot ductility of cast ATI®718Plus®: Effect of niobium and minor elements on liquation characteristics [J]. Materials Science and Engineering A, 2021, 799: 140151.

[20] XU Xiao-yan, MA Xiang-dong, WANG Hong, YE Zhang, CHANG Jian-wei, XU Yao, SUN Guang-ai, LÜ Wei-jie, GAO Yu-kui. Characterization of residual stresses and

microstructural features in an Inconel 718 forged compressor disc [J]. Transactions of Nonferrous Metals Society of China, 2019, 29: 569−578.
[21] LI Qi, XIE Jun, YU Jin-jiang, SHU De-long, HOU Gui-chen, SUN Xiao-feng, ZHOU Yi-zhou. Solidification behavior and segregation characteristics of high W content cast Ni based superalloy K416B [J]. Journal of Alloys and Compounds, 2020, 854: 156027.
[22] SHI Zhao-xia, DONG Jian-xin, ZHANG Mai-cang, ZHENG Lei. Solidification characteristics and segregation behavior of Ni-based superalloy K418 for auto turbocharger turbine [J]. Journal of Alloys and Compounds, 2013, 571: 168−177.
[23] WANG F, MA D, ZHANG J, BOGNER S, POLACZEK A B. Solidification behavior of a Ni-based single crystal CMSX-4 superalloy solidified by downward directional solidification process [J]. Materials Characterization, 2015, 101: 20−25.
[24] GONG Li, CHEN Bo, ZHANG Long, MA Ying-che, LIU Kui. Effect of cooling rate on microstructure, microsegregation and mechanical properties of cast Ni-based superalloy K417G [J]. Journal of Materials Science and Technology, 2018, 34: 811−820.
[25] YOU Xiao-gang, TAN Yi, SHI Shuang, YANG Jenn-ming, WANG Yi-nong, LI Jia-yan, YOU Qi-fan. Effect of solution heat treatment on the precipitation behavior and strengthening mechanisms of electron beam smelted Inconel 718 superalloy [J]. Materials Science and Engineering A, 2017, 689: 257−268.
[26] LONG Yi-tong, NIE Pu-lin, LI Zhu-guo, HUANG Jian, LI Xiang, XU Xin-mei. Segregation of niobium in laser cladding Inconel 718 superalloy [J]. Transactions of Nonferrous Metals Society of China, 2012, 22: 2106−2111.
[27] BISWAS S, REDDY G M, MOHANDAS T, MURTHY C V S. Residual stresses in Inconel 718 electron beam welds [J]. Journal of Materials Science, 2004, 39: 6813−6815.
[28] WANG Chang-shuai, WANG Ting-ting, TAN Mei-lin, GUO Yon-gan, GUO Jian-ting, ZHOU Lan-zhang. Thermal stability of a new Ni−Fe−Cr base alloy with different Ti/Al ratios [J]. Journal of Materials Science and Technology, 2015, 31: 135−142.
[29] MOHAMMAD J S, HAMED M, MOHSEN R. Solidification behavior and Laves phase dissolution during homogenization heat treatment of Inconel 718 superalloy [J]. Vacuum, 2018, 154: 235−243.
[30] MOHAMMAD J S, HAMED M. Unexoected formation of delta phase in as-cast niobium-bearing superalloy at solution annealing temperatures [J]. Materials Letters, 2020, 261: 127008.
[31] MOHAMMAD J S, HAMED M. Revisiting the diffusion of niobium in an as-cast nickel-based superalloy during annealing at elevated temperatures [J]. Metals and Materials International, 2020, 26: 326−332.
[32] ASALA G, KHAN A K, ANDERSSON J, OJO O A. Microstructural analyses of ATI 718Plus® produced by wire-ARC additive manufacturing process [J]. Metallurgical and Materials Transactions A, 2017, 48: 4211−4228.
[33] GENG C Y, WANG C Y, YU T. Site preference and alloying effect of platinum group metals in Ni_3Al [J]. Acta Materialia, 2004, 52: 5427−5433.
[34] KARUNARATNE M S A, REED R C. Interdiffusion of the platinum group metals in nickel at elevated temperatures [J]. Acta Materialia, 2003, 51: 2905−2919.
[35] CAO Wei-di. Solidification and solid state phase transformation of Allvac 718Plus alloy [C]//Superalloys 718, 625, 706 and Derivatives. New York: TMS, 2005: 165−177.
[36] GHOSH D C, CHAKRABORTY T. Gordy's electrostatic scale of electronegativity revisited [J]. Journal of Molecular Structure: Theochem, 2009, 906: 87−93.
[37] TRIPATHI S N, BHARADWAJ S R, DHARWADKAR S R. The Nb−Pt (niobium−platinum) system [J]. Journal of Phase Equilibria, 1995, 16: 465−470.
[38] SEEBOLD R E, BIRKS L S. Elevated temperature diffusion in the systems Nb−Pt, Nb−Se, Nb−Zn, Nb−Co, Ni−Ta, and Fe−Mo [J]. Journal of Nuclear Materials, 1961, 3: 260−266.
[39] CHEN Juan, XIAO Jin-kun, ZHANG Li-jun, DU Yong. Interdiffusion in fcc Ni−X (X = Rh, Ta, W, Re and Ir) alloys [J]. Journal of Alloys and Compounds, 2016, 657: 457−463.
[40] LIU Shao-hua, WEN Min-ru, LI Zi, LIU Wen-qing, YAN Ping, WANG Chong-yu. Partitioning and diffusion of transition metal solutes in ternary model Ni-based single crystal superalloys [J]. Materials & Design, 2017, 130: 157−165.

含 Pt 718Plus 高温合金的凝固行为

沈 宇[1,2,3]，王民庆[3]，夏 辉[1]，郑 磊[1]，孟 晔[4]，崔凤娥[4]

1. 北京科技大学 材料科学与工程学院，北京 100083；2. 北京钢研高纳科技股份有限公司，北京 100081；
3. 钢铁研究总院 高温合金部，北京 100081；4. 北京科技大学 新材料与技术研究院，北京 100083

摘 要：采用扫描电子显微镜(SEM)、能谱仪(EDS)、差示扫描量热法(DSC)和模拟计算研究含 Pt 高温合金 718Plus 的凝固行为。结果表明：Pt 的添加通过增加 Nb 的溶解度、扩大 γ 相区范围来降低合金的固相线温度和 Laves + γ 共晶相的析出温度，从而增大凝固范围。Pt 偏析于枝晶间区域，Pt 与 Nb/Ti 间强吸引的相互作用使枝晶间 Nb 和 Ti 的偏析增加，因此促进 Laves + γ 共晶相及其周围 η 相的析出。Pt 添加导致的凝固范围增大、Nb 和 Al 的偏析程度的增加促进共晶相附近 $\gamma'+\gamma''$相的析出和长大。这些结果为理解 Pt 在高温合金凝固行为中的作用机理提供了实验依据。

关键词：铂；凝固行为；718Plus 高温合金；共晶

(Edited by Wei-ping CHEN)